Available online at www.sciencedirect.com
ScienceDirect
Comput. Methods Appl. Mech. Engrg. 342 (2018) 458–473
Computer methods in applied mechanics and engineering
www.elsevier.com/locate/cma

Thermomechanical total Lagrangian SPH formulation for solid mechanics in large deformation problems

Kadiata Ba*, Augustin Gakwaya

Applied sciences Department, Université du Québec à Chicoutimi (UQAC), 555 boul. Université, Chicoutimi, Québec, Canada G7H 2B1
Mechanical Engineering Department, Université Laval, 1065 Avenue de la Médecine, Québec, Canada G1V 0A6

Received 10 May 2018; received in revised form 26 July 2018; accepted 27 July 2018
Available online 8 August 2018

Abstract

Challenging problems of computational mechanics may often be characterized by large deformations that are common in manufacturing processes such as forging. The finite element method faces difficulties in simulating large deformations, due to severe mesh distortion. A solution to overcome these difficulties is to use meshless methods like Smoothed Particle Hydrodynamics (SPH). This paper presents a thermomechanical SPH in total Lagrangian formulation to simulate efficiently large deformations thermomechanical problems. The continuum is modeled as a Hamiltonian system of particles (energy-based framework) when dissipative effects are considered where the constitutive equation is represented via an internal energy term. A comparison with an Eulerian SPH formulation and FEM is presented to assess the accuracy of the total Lagrangian formulation through examples of high velocity Taylor impact test and hot forging test.

Keywords: SPH; Eulerian; Total Lagrangian; Thermomechanical; Large deformations; Abaqus

1. Introduction

To overcome the limitations of the finite element method (FEM) in some operations involving fast dynamics, such as high-speed machining, large deformations or "flash" generation in forging, the Smoothed Particle Hydrodynamics method (SPH) is often used as an alternative to FEM.

SPH [1–5] was introduced in the 1970s by Lucy, Gingold and Monaghan [6–9]. The aim of this method which is one of the first numerical particle methods in mechanics [10] was to simulate phenomena such as the formation and evolution of stars and galaxies. Subsequently, it was applied to simulate applications in fluid dynamics (simulation of compressible, incompressible and multiphase fluids, etc.).

The extension of the method to structural mechanics is more recent (in the 1990s). Libersky and Petschek [11] and Libersky et al. [4] are cited as the first to use SPH in solid mechanics, for the modeling of impacts at high speeds

* Corresponding author at: Applied sciences Department, Université du Québec à Chicoutimi (UQAC), 555 boul. Université, Chicoutimi, Québec, Canada G7H 2B1.
E-mail address: kadiata_ba@uqac.ca (K. Ba).

https://doi.org/10.1016/j.cma.2018.07.038
0045-7825/

and phenomena of rupture, perforation and fragmentation. Since there is no mesh to distort, the method can handle large deformations. Applications in forging processes [12], machining [13–15] and welding [16] position SPH as an efficient numerical method for the simulation of mechanical shaping problems. Indeed, compared to FEM, SPH presents several advantages:

- No fixed connectivity between the nodes, which eliminates the undesirable meshing effects (mesh distortion).
- Great ability to follow the surface deformations.
- Ability to model complex problems and geometries.

Although advantages like the no mesh distortion and the ability to interact with complex geometry are interesting, it should be noted that SPH faces certain numerical problems in particular the problems of numerical integration when a weak formulation is used, the problems of tensile instability (nodal integration is the origin of well known instabilities in meshless methods), lack of consistency, free boundary and the zero energy modes problems. While modeling forging or machining processes using SPH, a big challenge is often the tensile instability specially when using an Eulerian code. Corrections are required for efficient treatment, but are not necessarily available in commercial codes such as Abaqus.

Several works have been done to overcome some of these limitations. Corrections and new formulations were proposed by authors to get more accuracy. In that regard, to improve the accuracy for free boundaries, Johnson and Beissel [17] proposed an approach that consists of adjusting the standard smoothing functions for every node (and every cycle) such that the normal strain rates are computed exactly for conditions of constant strain rates improving the accuracy for non-uniform strain rates. Dyka et al. [18] and Randles and Libersky [19] contributed to the correction of the tensile instability through stress-point that stabilizes the method, a companion set of Lagrangian points that carry the stress, velocity gradient, and other derived field variables. Ganzenmüller et al. [20] proposed to correct zero energy modes problems by using the same approach as in the correction of hourglass mode in FEM. For the tensile instability, many corrections were proposed by using MLS (moving least squares) functions [21]. Chen et al. [22] also proposed a correction of the SPH method, which improves the consistency properties of shape functions. There is also the approach adopted by Belytschko et al. [23] which consists in using a total Lagrangian formulation to eliminate some problems of tensile instability. In [23], convergence studies using both Eulerian and Lagrangian kernels demonstrated that problems of tensile instability arise because the SPH approach is Lagrangian by construction, the use of an Eulerian kernel reveals an instability when the particles are in a state of tension (the use of total Lagrangian kernel cured the tensile instability problems but not the zeros energy modes problem). The use of the total Lagrangian formulation also makes it possible to reduce the CPU time by avoiding the search for neighboring particles for the construction of the kernel function at each time step, the particles remaining mainly adjacent along in solid mechanics process. Regarding new formulations, Farrokhpanah et al. [24] present an approach for modeling heat conduction, which uses smoothing, and superposition of two kernels to gradually release/absorb the latent heat near the phase change temperature. Vidal et al. [25] present a stabilized updated Lagrangian corrected SPH for explicit dynamic problems to handle problems with extremely large distortions.

This paper presents a thermomechanical total Lagrangian SPH formulation more adapted to solid mechanics for large deformation problems such as forging and high velocity impact. The works were done in two steps: (a) first, an in-house code is developed in FORTRAN; (b) and second, an extension to a VUEL subroutine (user's element) for Abaqus user. In fact, when it comes to using SPH for modeling solid materials the choice is limited. Abaqus includes the SPH formulation but with reduced functionality (Eulerian formulation only). Then, this second contribution is to help to improve the use of SPH in Abaqus.

Hamiltonian formulation (weak energy formulation) is also presented. Compared to a classical strong formulation based on differential equations, this formulation is responsible for the long-term stability.

Applied to simulate some challenging thermomechanical problems, the results of this formulation are compared to those obtained using the Eulerian SPH approach implemented in Abaqus to verify the accuracy of the implemented algorithm and to see if it does suffer from classical SPH drawbacks such as consistency or tensile instability?

2. Thermomechanical formulation

The present work considers a coupled thermomechanical analysis. The problem is then described by the following conservation laws. Let us introduce φ, the deformation mapping. It maps every particle $\mathbf{X}$ of the undeformed reference configuration Ω_0 to its deformed counterpart $\mathbf{x}$ at time t belonging to the current configuration Ω_t.

o Mass conservation :

$$\rho_0 = \rho J = \rho \det \mathbf{F}$$
$$\mathbf{F} = \text{grad}\varphi = \frac{\partial \mathbf{x}}{\partial \mathbf{X}} \tag{1}$$

where ρ_0 and ρ are initial and current densities of volume elements, J is the Jacobian and $\mathbf{F}$ is the deformation gradient.

o Momentum conservation:

$$\rho_0 \mathbf{a} = \frac{\partial}{\partial \mathbf{X}} \mathbf{P} + \rho_0 \mathbf{f}_0 \tag{2}$$

where $\mathbf{a}$ is the acceleration, $\mathbf{f}_0$ is body force per unit mass, $\mathbf{P}$ is the first Piola–Kirchhoff stress tensor and $\frac{\partial}{\partial \mathbf{X}}$ the divergence operator.

Boundary conditions are required in order to solve Eq. (2). With the disjunct decomposition $\partial\Omega_0 = \partial\Omega_{0,\varphi} \cup \partial\Omega_{0,\mathbf{t}}$ of the boundary $\partial\Omega_0$, the boundary conditions are:

$$\varphi = \overline{\varphi} \quad \forall \mathbf{X} \in \partial\Omega_{0,\varphi}$$
$$\mathbf{P}.\mathbf{n} = \bar{\mathbf{t}} \quad \forall \mathbf{X} \in \partial\Omega_{0,\mathbf{t}} \tag{3}$$

where $\mathbf{n}$ is the normal vector at the boundary, $\overline{\varphi}$ is the prescribed deformation associated with the boundary $\partial\Omega_{0,\varphi}$ and $\bar{\mathbf{t}}$ is the prescribed tractions associated with the boundary $\partial\Omega_{0,\mathbf{t}}$.

o Energy conservation:

The thermomechanical problem is coupled by considering the following effects:

1. Heat generation by the plastic dissipation.
2. Contribution of the thermal expansion to the total material deformation.
3. Influence of the temperature on the yield stress of the material.

$$\rho_0 \dot{E} = \mathbf{P} : \dot{\mathbf{F}} - div\mathbf{H} + Q_T + R_{pl} \tag{4}$$

where E is the internal energy per unit mass, $\mathbf{F}$ is the deformation gradient, $\mathbf{H}$ is the heat flux, Q_T is the internal heat source and R_{pl} the mechanical contribution.

The boundary conditions to solve Eq. (4) are:

$$T = \overline{T} \quad \forall \mathbf{X} \in \partial\Omega_{0,T}$$
$$\mathbf{H}.\mathbf{n} = \overline{H} \quad \forall \mathbf{X} \in \partial\Omega_{0,H} \tag{5}$$

where $\overline{T}$ are prescribed temperatures associated with the boundary $\partial\Omega_{0,T}$ and $\overline{H}$ is a prescribed heat flux corresponding to the boundary $\partial\Omega_{0,H}$.

The mechanical contribution r_{pl} (heat generation by the plastic dissipation) given by the classical Taylor–Quinney hypothesis is:

$$R_{pl} = \beta \sigma_{eq}^{y} \Delta \varepsilon_{eq}^{p} \tag{6}$$

where ε_{eq}^{p} is the equivalent plastic deformation, β represents the fraction of the mechanical energy transformed into heat, σ_{eq}^{y} is the actual (equivalent) flow stress of the material given by the flow law.

o Balance law of entropy or second law of thermodynamics

The second law of thermodynamics specifies that the net entropy production within Ω_0 must be non-negative:

$$D = T\dot{S} = T\dot{N} - \dot{E} + \mathbf{P} : \dot{\mathbf{F}} + \mathbf{H} \cdot \mathbf{G} \geq 0 \tag{7}$$

where N being the entropy, $\dot{S}$ the internal entropy production and

$$G = -\frac{1}{T} \text{grad} T \tag{8}$$

being the normalized temperature gradient. It represents the driving force and energetically conjugate variable to the heat flux $\mathbf{H}$. Often, the dissipation D is decomposed into the internal dissipation D_{int} and the dissipation due to heat conduction D_{cond} [26]:

$$D_{\text{int}} = T\dot{N} - \dot{E} + \mathbf{P} : \dot{\mathbf{F}} \tag{9}$$
$$D_{cond} = \mathbf{H} \cdot \mathbf{G} \tag{10}$$

Following the assumption that the thermal problem can be described by a Fourier-type constitutive model, the dissipation due to heat conduction is non-negative ($D_{cond} \geq 0$) and the second law of thermodynamics is automatically fulfilled, if the internal dissipation is non-negative ($D_{\text{int}} \geq 0$). Then, Eq. (7) is verified ($D = T\dot{N} - \dot{E} + \mathbf{P} : \dot{\mathbf{F}} - \frac{\mathbf{H}}{T}\text{grad}T \geq 0$)

In line with Canadija and Mosler [26], the internal energy and the Helmholtz energy, together with their restrictions imposed by the second law of thermodynamics are given by:

$$E = E\left(\mathbf{F}, N, \boldsymbol{\alpha}\right) \tag{11}$$

where $\boldsymbol{\alpha}$ is a set of suitable strain-like internal variables associated with the deformation history.

$$\Psi = \Psi\left(\mathbf{F}, T, \boldsymbol{\alpha}\right) \tag{12}$$

This transformation requires already the definition of the temperature T as energetically conjugate to the entropy N, i.e., $T = \partial_N E$. By substituting Eq. (12) into Eq. (7), the total dissipation can be re-written as

$$D = \left[-N - \frac{\partial \Psi}{\partial T}\right]\dot{T} + \left[\mathbf{P} - \frac{\partial \Psi}{\partial \mathbf{F}}\right] : \dot{\mathbf{F}} - \frac{\partial \Psi}{\partial \alpha} : \dot{\boldsymbol{\alpha}} - \frac{\mathbf{H}}{T}\text{grad}T \geq 0 \tag{13}$$

Accordingly to a fully reversible loading process, the state equations (Eqs. (14) and (15)) can be derived:

$$\mathbf{P} = \partial_{\mathbf{F}} \Psi \tag{14}$$

$$N = -\partial_T \Psi \tag{15}$$

Applied to Eq. (13), it yields the reduced internal dissipation

$$D = -\frac{\partial \Psi}{\partial \alpha} : \dot{\boldsymbol{\alpha}} - \underbrace{\frac{\mathbf{H}}{T}\text{grad}T}_{thermal-dissipation} \geq 0 \tag{16}$$

The evolution equations $\dot{\boldsymbol{\alpha}}$ have to be chosen in line with the second law of thermodynamics.

In line with Canadija and Mosler [26] and Mosler and Bruhns [27] for elastoplasticity material models, it is convenient to decompose the set of internal variables $\boldsymbol{\alpha}$ into the plastic strains (the plastic part of the deformation gradient $\mathbf{F}^p$), a strain-like second order tensor $\boldsymbol{\alpha}_k$ associated with kinematic hardening and its isotropic counterpart α_i. As a result, $\boldsymbol{\alpha} = \{\mathbf{F}, \boldsymbol{\alpha}_k, \alpha_i\}$ and thus, the Helmholtz energy becomes $\Psi = \Psi\{\mathbf{F}^e, T, \boldsymbol{\alpha}_k, \alpha_i\}$ and:

$$\begin{aligned} &D = \sum : \mathbf{L}^p + \mathbf{Q}_k : \dot{\boldsymbol{\alpha}}_k + Q_i\dot{\alpha}_i - \frac{\mathbf{H}}{T}\text{grad}T \geq 0, \\ &\mathbf{Q}_k = -\partial_{\alpha_k} \Psi \\ &Q_i = -\partial_{\alpha_i} \Psi \end{aligned} \tag{17}$$

where $\mathbf{Q}_k$ and Qi are stress-like internal variables conjugate to $\boldsymbol{\alpha}_k$ and α_i, $\mathbf{L}^p = \dot{\mathbf{F}^P} \cdot [\mathbf{F}^p]^{-1}$ is the plastic velocity gradients and $\sum = \mathbf{F}^{eT} \cdot \partial_{F^e} \Psi$ are the Mandel stresses.

The temperature variation can be determined by combining Eq. (17) with the energy conservation equation:

$$c\dot{T} = q_T + r_{pl} - div\mathbf{H} + D + T\partial^2_{T\mathbf{F}^e} \Psi : \dot{\mathbf{F}^e} \tag{18}$$

where c is the heat capacity.

3. Discrete equations of motion from energy-based formulation

An energy-based approach (Hamiltonian) is applied to build a new set of discrete equations [28–30]. In this energy-based framework, the solid is discretized into a finite number of particles and the motion of each particle is given by the classical Lagrange equations. This procedure of deriving the governing equations bypasses the standard differential equations of equilibrium and ensures that the constants of the motion such as linear and angular momentum are preserved [29]. The relevant physical quantities on each particle are calculated by an interpolation process over neighboring particles. Every particle is regarded as a moving thermodynamic subsystem with a mass m_i, position $\mathbf{x}_i$ and velocity $\mathbf{v}_i$, density ρ_i, and volume $V_i = m_i/\rho_i$. To proceed with a variational formulation of the equations of

motion of the continuum, it is necessary to define the kinetic, internal and external energy of the system. The total kinetic energy of the system can be approximated as the sum of the kinetic energy of each particle:

$$K = \frac{1}{2}\sum_i m_i \left(\mathbf{v}_a.\mathbf{v}_a\right) \tag{19}$$

Similarly, for a common case where the external forces result from a gravitational field $\mathbf{g}$, the total external energy is:

$$\prod_{ext} = -\sum_i m_i \left(\mathbf{x}_a.\mathbf{g}\right) \tag{20}$$

The total internal energy can be expressed as the sum of the products of particle masses by the amount of energy accumulated per unit mass π which depend on the deformation, density or other constitutive parameters:

$$\prod_{int} = \sum_i m_i \pi \left(\rho_i, \ldots\right) \tag{21}$$

With dissipative effects such as plasticity and viscous flow, the equations of motion of the system of particles representing the continuum can now be evaluated following the classical Lagrangian formalism

$$\frac{d}{dt}\frac{\partial L}{\partial \mathbf{v}_i} - \frac{\partial L}{\partial \mathbf{x}_i} = -\frac{\partial \Pi_{dis}}{\partial \mathbf{v}_i} \tag{22}$$

$$L\left(\mathbf{x}_i, \mathbf{v}_i\right) = K\left(\mathbf{v}_i\right) - \Pi_{ext}\left(\mathbf{x}_i\right) - \Pi_{int}\left(\mathbf{x}_i\right) \tag{23}$$

Substituting Eqs. (19)–(21) into Eq. (22) leads to:

$$\frac{d}{dt}\frac{\partial K}{\partial \mathbf{v}_i} = -\frac{\partial \Pi_{ext}}{\partial \mathbf{x}_i} - \frac{\partial \Pi_{int}}{\partial \mathbf{x}_i} - \frac{\partial \Pi_{dis}}{\partial \mathbf{v}_i} \tag{24}$$

which can be expressed as the Newton's second law for each particle as:

$$m_i \mathbf{a}_i = \underset{\text{gravity}}{F_i^{grav}} - \underset{\text{internal}}{F_i^{int}} - \underset{\text{dissipative}}{F_i^{dis}} \tag{25}$$

The subsequent work will develop the momentum conservation with:

$$\begin{aligned} \frac{d\mathbf{v}_i}{dt} = \mathbf{a}_i = \; & \underset{gravity}{\mathbf{a}_i^g} + \underset{\text{internal}}{\mathbf{a}_i^{int}} + \underset{dissipative}{\mathbf{a}_i^{dis}} \\ \underset{\text{internal}}{\mathbf{a}_i^{int}} = \; & \underset{volumetric}{\mathbf{a}_i^{vol}} + \underset{deviatoric}{\mathbf{a}_i^{dev}} \end{aligned} \tag{26}$$

where the acceleration due to the internal potential energy is made of a volumetric and deviatoric part. In the case of gravity, the acceleration can be easily computed as:

$$\mathbf{a}_i^g = \frac{F_i}{m_i} = -\frac{1}{m_i}\frac{\partial \Pi_{ext}}{\partial \mathbf{x}_i} = -\frac{1}{m_i}\left(-m_i \mathbf{g}\right) = \mathbf{g} \tag{27}$$

and the acceleration due to the volumetric part of internal energy is:

$$\mathbf{a}_i^{vol} = \sum_{j=1}^{N} m_j \left(\frac{\beta_j' p_j}{\rho_j^2} + \frac{\beta_i' p_i}{\rho_i^2}\right) \nabla W_{ij} \tag{28}$$

$$\beta_i' = \left[-\frac{1}{d_m \rho_i}\sum_{j=1}^{N} m_j r_{ij}\frac{\partial W_{ij}}{\partial r_{ij}}\right]^{-1} \tag{29}$$

In case of elasticity, the internal strain energy includes both a volumetric and a deviatoric part, which depends on the constitutive law of the material due to shear such that:

$$\sigma^{\alpha\beta} = -p\delta^{\alpha\beta} + \tau^{\alpha\beta} \tag{30}$$

The contribution of the pressure to the constitutive law has already been taken into account by the volumetric internal energy. A deviatoric potential, π_{dev} can be defined as the rate of energy dissipated by the deviatoric forces per unit volume. This makes it possible to define the deviatoric internal energy as:

$$\Pi_{dev} = \sum_{i=1}^{Ntot} m_i \pi_{dev}(\mathbf{d}) \tag{31}$$

and the viscous potential relates to the shear stress as follows:

$$\tau^{\alpha\beta} = \rho \frac{\partial \pi_{dev}(\mathbf{d})}{\partial \mathbf{d}} \tag{32}$$

Hence, the associated internal force is:

$$F_i^{dev} = \frac{\partial (\Pi_{dev})_i}{\partial \mathbf{v}} = m_i \frac{\partial (\Pi_{dev})_i}{\partial \mathbf{d}} \frac{\partial \mathbf{d}}{\partial \mathbf{v}} \tag{33}$$

The rate of deformation tensor $\mathbf{d}$ is defined in terms of velocity $\mathbf{v}$ as:

$$\mathbf{d} = \frac{1}{2}\left(\nabla \mathbf{v} + \nabla \mathbf{v}^T\right) \cong \frac{1}{2}\left(\sum_{j=1}^{n} \frac{m_j}{\rho_j} \mathbf{v}^{\alpha} \cdot \frac{\partial W_{ij}}{\partial \mathbf{x}^{\beta}} + \sum_{j=1}^{n} \frac{m_j}{\rho_j} \mathbf{v}^{\beta} \cdot \frac{\partial W_{ij}}{\partial \mathbf{x}^{\alpha}}\right) \tag{34}$$

and its derivative with respect to $\mathbf{v}$ is:

$$\frac{\partial \mathbf{d}}{\partial \mathbf{v}} = \frac{1}{2}\left(\sum_{j=1}^{n} \frac{m_j}{\rho_j} 1 \cdot \frac{\partial W_{ij}}{\partial \mathbf{x}^{\beta}} + \sum_{j=1}^{n} \frac{m_j}{\rho_j} 1 \cdot \frac{\partial W_{ij}}{\partial \mathbf{x}^{\alpha}}\right) = \sum_{j=1}^{n} \frac{m_j}{\rho_j} \nabla W_{ij} \tag{35}$$

Using Eqs. (32) and (35), it is possible to write the acceleration resulting from the deviatoric stresses as:

$$\mathbf{a}_i^{dev} = \frac{F_i^{dev}}{m_i} = \sum_{j=1}^{n} \frac{m_j}{\rho_i \rho_j} \left(\tau^{\alpha\beta}\right)_j \nabla W_{ij} \tag{36}$$

From Eq. (17), it is possible to express the dissipative energy as:

$$\Pi_{disp} = \sum_i \left(\sigma : \mathbf{d}^p + q_k : \dot{\boldsymbol{\alpha}}_k + q_i \dot{\alpha}_i - \frac{h}{T} \mathrm{grad} T\right) \geq 0 = \sum_{i=1}^{Ntot} m_i \pi_{disp}(\mathbf{d}) \tag{37}$$

where $\pi_{disp}(\mathbf{d})$ is dissipative energy per unit mass. The resulting acceleration component is therefore given by:

$$\begin{aligned} &\mathbf{a}_i^{disp} = \frac{F_i^{disp}}{m_i} = \sum_{j=1}^{n} \frac{m_j}{\rho_i \rho_j} \left(\tau^{\alpha\beta}\right)_j \nabla W_{ij} \\ &with \\ &\tau^{\alpha\beta} = \rho \frac{\partial \pi_{disp}(\mathbf{d})}{\partial \mathbf{d}} \end{aligned} \tag{38}$$

4. Corrected total Lagrangian SPH formulation for solid mechanics

In solids mechanics, SPH particles change less often theirs neighbors than in fluid mechanics. This is why a total Lagrangian formulation [31,32] is well suited. The material coordinates $\mathbf{X}$ are used instead of the spatial coordinates $\mathbf{x}$, the SPH kernels and their gradients are then expressed in the initial configuration.

In order to address the lack of completeness and interpolation consistency, corrected kernel has been implemented. In this work, the smoothing length h is considered as a functional variable in the calculation of the gradient of the kernel function [30].

Considering a general deformation of a body discretized using a number of SPH particles, the deformation gradient defined in Eq. (1) can now be evaluated at a given particle i in terms of the current particle positions as:

$$\mathbf{F}_i = \sum_{j=1}^{n} \mathbf{x}_j \otimes \mathbf{G}_j(\mathbf{X}_i) \tag{39}$$

where G is the gradient function and contains the corrected kernel gradients $\widetilde{\nabla} W(\mathbf{X})$ at the initial reference configuration. The kernel gradient vector G is given by:

$$\mathbf{G}_i\left(\mathbf{X}_j\right) = V_i \widetilde{\nabla}_0 \mathbf{W}_i\left(\mathbf{X}_j\right) \tag{40}$$

Note that **G** is computed at the beginning of the problem and does not change since the neighbors will be the same throughout the numerical calculation, which will help to reduce the computational cost.

A common correction is the symmetrization introduced by Monaghan [7]. When used for deformation gradient, it yields:

$$\mathbf{F}_i = \sum_{j=i}^{n} \left(\mathbf{x}_j - \mathbf{x}_i\right) \mathbf{G}_j\ \left(\mathbf{X}_i\right) \tag{41}$$

The expression of the corrected deformation gradient, in total Lagrangian formulation, is then written:

$$\langle \mathbf{F}_i \rangle = \left(-\sum_j \left(\mathbf{u}_j - \mathbf{u}_i\right) \otimes \nabla_{\mathbf{X}_j} W\left(\mathbf{X}_i - \mathbf{X}_j, h_0\right) V_j^0 \right) \mathbf{B} + I \tag{42}$$

The expression of the correction of the gradient is given by [31]:

$$\mathbf{B} = \left(\sum_j \frac{m_j}{\rho_j} \left(\mathbf{X}_i - \mathbf{X}_j, h_0\right) \otimes \nabla_{\mathbf{X}_i} W\left(\mathbf{X}_i - \mathbf{X}_j, h_0\right) \right)^{-1} \tag{43}$$

The corrected momentum equation for a particle i is given by:

$$\langle \mathbf{a}_i \rangle = \left(-\sum_j \left(\mathbf{P}_j - \mathbf{P}_i\right) \otimes \nabla_{\mathbf{X}_j} \widetilde{W}\left(\mathbf{X}_i - \mathbf{X}_j, h_0\right) V_j^0 + \mathbf{f}_i \right) : \mathbf{B} \tag{44}$$

where **P** is the first Piola–Kirchhoff stress that will be determined by following the following process:

- In the Lagrangian formulation, the Green–Lagrange deformation tensor is used as deformation measurement expressed in terms of the strain gradient as follows:

$$\mathbf{E} = \frac{1}{2}\left(\mathbf{F}^T\mathbf{F} - \mathbf{I}\right) \tag{45}$$

- By taking the derivative with respect to the time of the tensor of Green–Lagrange, Eq. (45) becomes :

$$\dot{\mathbf{E}} = \frac{1}{2}\left(\mathbf{F}^T\dot{\mathbf{F}} + \dot{\mathbf{F}}^T\mathbf{F}\right) \tag{46}$$

- The rate of change of Green–Lagrange's material deformation tensor and the spatial deformation rate tensor **D** are related by the following convective transport relation:

$$\mathbf{D} = \left(\mathbf{F}^{-T}\dot{\mathbf{E}}\mathbf{F}^{-1}\right) \tag{47}$$

which is the measure of the deformation used to update the Cauchy stress rates written in a corotational frame. The constraint is then integrated incrementally in time [31]:

$$\sigma_{ij}\left(t + dt\right) = \sigma_{ij}\left(t\right) + \dot{\sigma}_{ij} dt = \sigma_{ij}\left(t\right) + \left(\sigma_{ij}^{\nabla} + \sigma_{ik}R_{kj} + \sigma_{jk}R_{kl}\right) dt \tag{48}$$

with $\sigma_{ij}^{\nabla} = C_{ijkl}D_{kl}$ also called Jaumann constraint rate (to respect objectivity), R is the spin tensor and C_{ijkl} is the material tangent modulus.

- The Cauchy stress must now be transformed into the first Piola–Kirchhoff stress by the relation:

$$\mathbf{P} = J\boldsymbol{\sigma}\mathbf{F}^{-T} \tag{49}$$

The corrected energy conservation equation particle i is given by:

$$\left\langle \dot{\mathbf{e}}_i \right\rangle = \mathbf{P}_j : \left[\left(-\sum_j \frac{m_j}{\rho_i \rho_j} \left(\mathbf{v}_j - \mathbf{v}_i, h_0\right) \otimes \nabla_{\mathbf{X}_i} W\left(\mathbf{X}_i - \mathbf{X}_j, h_0\right) V_j^0 + k\nabla T_i + r_{pl} \right) \mathbf{B} \right] \tag{50}$$

Eqs. (44) and (50) are respectively the equation of motion and the equation of the thermal energy of each particle which can be put after discretization and evaluation of all the interactions in the forms:

$$\begin{aligned} \mathbf{a}_i = \ddot{\mathbf{u}}_i &= \frac{1}{\mathbf{m}_i}(\mathbf{f}_{ext(i)} - \mathbf{f}_{\text{int}(i)}) \\ \dot{\mathbf{T}}_i &= \frac{1}{\mathbf{c}_i}(\mathbf{h}^k_{ext(i)} - \mathbf{h}^k_{int(i)}) \end{aligned} \tag{51}$$

where $\mathbf{f}_{\text{int}(i)}$ and $\mathbf{f}_{ext(i)}$ are the internal and external forces and $\mathbf{h}^k_{int(i)}$ and $\mathbf{h}^k_{ext(i)}$ are the internal and the external heat flux.

The expression for the internal force for a given particle can be expressed by differentiating the internal energy per unit mass with respect to nodal positions as:

$$\mathbf{f}_{\text{int}(i)} = \sum_{j=1}^{n} V_j^0 \mathbf{P}_j \, \mathbf{G}_i \left(\mathbf{X}_j\right) \tag{52}$$

Internal heat flux can be expressed as $\mathbf{h}_{int(i)} = \mathbf{k}_i \mathbf{T}_i$, $\mathbf{k}$ being the heat conductivity matrix, and $\mathbf{T}$ the vector of nodal temperatures.

These differential equations are solved numerically by an explicit finite difference method used in explicit dynamics to update the velocity, position and temperature of each SPH particle.

5. Temporal integration scheme

5.1. In-house code

A typical integration scheme used for integrating SPH equations is the leap-frog algorithm [31]. This algorithm is an extension of the Verlet algorithm and has the advantage of a low storage memory during computation. At the beginning of the integration (first step of the simulation), it is considered that $\Delta t^n = \Delta t^{n+1}$:

$$\overrightarrow{u}^{n-1/2} = \overrightarrow{u}^{n} - \frac{1}{2}\overrightarrow{v}^{n-1/2}\Delta t^n \tag{53}$$

At this point, the position of the particles and velocities are known at n-1/2. The deformation gradient and the tensor deformation rate of Green–Lagrange are calculated. After this, the position of the particles is updated:

$$\overrightarrow{u}^{n} = \overrightarrow{u}^{n-1/2} + \frac{1}{2}\overrightarrow{v}^{n-1/2}\Delta t^n \tag{54}$$

The deformation gradient is calculated again to calculate the Jacobian at n. The strain rate is calculated at $n - 1/2$ and the strain tensor is updated as follows:

$$\boldsymbol{\sigma}^n = \boldsymbol{\sigma}^{n-1} + \dot{\boldsymbol{\sigma}}^{n-1/2}\Delta t^n \tag{55}$$

The velocities are advanced over time by $n + 1/2$ using the following expression:

$$\overrightarrow{v}^{n+1/2} = \overrightarrow{v}^{n-1/2} + \Delta t^* \overrightarrow{a}^{n} \tag{56}$$

During the first step only:

$$\Delta t^* = \frac{1}{2}\left(\Delta t^n + \Delta t^{n+1}\right) \tag{57}$$

For the following steps:

$$\Delta t^* = \frac{1}{2}\left(\Delta t^{n+1}\right) = \frac{1}{2}\left(\Delta t^{n}\right) \tag{58}$$

Finally, the position of the particles is updated with the new speed:

$$\overrightarrow{u}^{n+1} = \overrightarrow{u}^{n} + \overrightarrow{v}^{n+1/2}\Delta t^{n+1} \tag{59}$$

The new time variable is assigned as follows:

$$\Delta t^n = \Delta t^{n+1} \tag{60}$$

At n + 1, the new time step is given by:

$$\Delta t^{n+1} = \Delta t_{crit} m \tag{61}$$

where m is a time scaling factor and the steady time is given by the CFL (Courant–Friedrichs–Levy) condition:

$$\Delta t_{crit} = \min\left(\frac{\Delta r_{\min}}{c_d}\right) \tag{62}$$

with c_d the speed of sound through the material.

The CFL condition shows that the computational domain in the digital simulation must include the physical domain, where the maximum digital propagation speed must be greater than the maximum physical propagation speed. This CFL condition requires a time step proportional to the smallest inter-particle distance $\Delta r_{\min}$ [16,33,34]. It should be noted that in practice, according to Timesli [16], the time step in SPH applications depends on the physical nature of the problem and may be greater than the one estimated using the CFL condition.

The forward Euler explicit time integration method has been implemented for the solution of the thermal problem in the numerical algorithm for the thermomechanical analysis.

$$\overrightarrow{T}^{n+1} = \overrightarrow{T}^{n} + \dot{\overrightarrow{T}}^{n} \Delta t^{n+1} \tag{63}$$

$\dot{\mathbf{T}}_t$ is computed after assembly as follows:

$$\dot{\overrightarrow{T}}^{n} = [\mathrm{C}]^{-1} \left([\mathrm{h}]_{ext} - [\mathrm{h}]_{\mathrm{int}}\right) \tag{64}$$

where [C] is the lumped thermal capacitance matrix based on the previous time step, $[\mathrm{h}]_{ext}$ is the applied nodal source vector, and $[\mathrm{h}]_{int}$ is the internal flux vector.

An approximation of the stability limit of the thermal solution is given by:

$$\Delta t_T \approx \frac{\Delta r^2_{\min}}{2\alpha} \tag{65}$$

where $\alpha = \frac{k}{\rho c}$ is the diffusivity of the material, k being the conductivity.

The new configuration $\overrightarrow{u}^{n+1}$ is obtained from the explicit equations of motion with the temperatures assumed fixed, and the new temperature $\overrightarrow{T}^{n+1}$ is calculated at constant geometry. The results are exchanged at each step and coupling terms are calculated.

5.2. VUEL

For the user element, the solution process is done by Abaqus using his explicit dynamic algorithm. The explicit dynamics analysis procedure in Abaqus/Explicit is based upon the implementation of an explicit integration rule together with the use of diagonal or "lumped" element mass matrices. Here is a summary of the explicit dynamics algorithm from Abaqus documentation [35] for the thermomechanical problem.

The heat transfer equations are integrated using the explicit forward-difference time integration rule.

$$\mathbf{T}_{(t+\Delta t)} = \mathbf{T}_{(t)} + \Delta t_{(t+1)} \dot{\mathbf{T}}_{(t)} \tag{66}$$

The values of $\dot{\mathbf{T}}_t$ are computed at the beginning of the increment by :

$$\dot{\mathbf{T}}_{(t)} = \mathbf{C}^{-1} \left(\mathbf{h}^t_{ext} - \mathbf{h}^t_{\mathrm{int}}\right) \tag{67}$$

The stability limit is given by:

$$\Delta t_T \approx \frac{L^2_{\min}}{2\alpha} \tag{68}$$

The mechanical problem is formulated in terms of nodal accelerations . The equations of motion (mechanical equilibrium) are integrated using the explicit central difference integration rule.

$$\ddot{\mathbf{u}}_{(t)} = \mathbf{M}^{-1} \left(\mathbf{P}_{(t)} - \mathbf{I}_{(t)}\right) \tag{69}$$

where $\ddot{\boldsymbol{u}}$ is the nodal acceleration at time t_n, $\mathbf{M}$ is the mass matrix, and $\mathbf{P}_{(t)}$ and $\mathbf{I}_{(t)}$ are the external and internal forces.

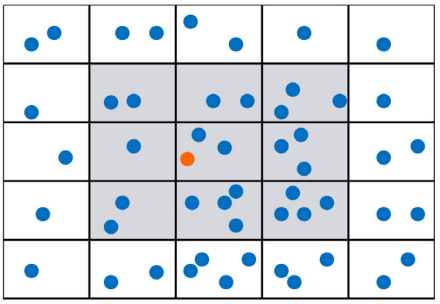

Fig. 1. Linked-list algorithm [37].

The explicit integrate explicitly leads to $\mathbf{u}_{(t+\Delta t)}$

$$\dot{\mathbf{u}}_{(t+\frac{\Delta t}{2})} = \dot{\mathbf{u}}_{(t-\frac{\Delta t}{2})} + \frac{\left(\Delta t_{(t+\Delta t)} + \Delta t_{(t)}\right)}{2}\ddot{\mathbf{u}}_{(t)} \tag{70}$$

$$\mathbf{u}_{(t+\Delta t)} = \mathbf{u}_{(t)} + \Delta t_{(t+\Delta t)}\dot{\mathbf{u}}_{(t+\frac{\Delta t}{2})} \tag{71}$$

The stability limit is given by:

$$\Delta t = \min\left(\frac{L_e}{c_d}\right) \tag{72}$$

where L_e is the characteristic element dimension and c_d is the current effective, dilatational wave speed of the material.

Since both the forward-difference and central-difference integrations are explicit, the heat transfer and mechanical solutions are obtained simultaneously by an explicit coupling.

6. Neighbor search

6.1. In-house code

The calculation time in SPH is an important aspect, since the method is generally disadvantaged for its long calculation time. This aspect is partly due to the management of the search for neighboring particles during the computation and the updating of the zone of influence of a particle. Indeed, the kernel function W is supposed to be supported compactly. This means that the number of neighbors is finite [36]. In order to calculate the value of $\nabla_i W_{ij}$ or W_{ij}, the neighbors of a particle must be known. To achieve this, the particles within a given radius must be found through a closest neighbor search algorithm. In total Lagrangian formulation, the particle neighbor is computed once at the beginning and stored in memory. The neighbor search algorithm used in the present work is the linked-list algorithm [3], which is more efficient than the all-pair search algorithm (all the particles of the domain are analyzed) and faster than the three search algorithm (the domain is divided into smaller subdomains that contain a single particle) [36]. Linked-list algorithm (Fig. 1) consists in dividing the domain in square cells of length hi and to sort the particles in its corresponding cell. When this is done, the neighbors of a particle are in neighboring cells. This limits the number of calculations of r_{ij}, its efficiency is estimated at O (N) if the number of particles per cell is quite low.

6.2. VUEL

In Abaqus, all particles are tracked as the analysis progresses, it is called the all-pair search algorithm (Fig. 2). It is less efficient, all the particles of the domain are analyzed and the inter-particle distances r_{ij} verified in order to find the neighbors of a particle. This leads to a calculation time of the order of N^2, where N is the total number of particles [36].

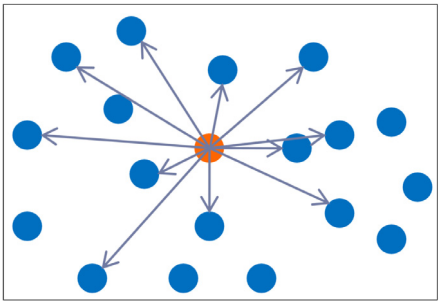

Fig. 2. All-pair search algorithm [37].

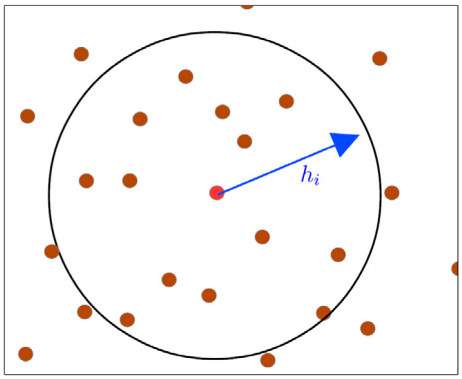

Fig. 3. SPH smoothing length representation [38].

7. User element description and implementation

The SPH user element has one node with six degrees of freedom at each node (Fig. 3). Each node continuum particle has three translational and three rotational degrees of freedom.

The element centered at a given node (particle) receives contributions from all particles within a sphere of influence whose radius is commonly referred to as the smoothing length *hi*.

Fig. 4 shows the flow chart of SPH method for the in-house code, FORTRAN is used for the whole coding.

Fig. 5 shows the logic diagram of the VUEL. The thermomechanical SPH element is written in FORTRAN and implemented in Abaqus Explicit version 6.14 using the VUEL subroutine that allows the user to calculate the whole discrete system: mass matrix, internal and external forces, behavior law based on a thermomechanical formulation nonexistent in Abaqus.

8. Applications: numerical examples

To assess the total Lagrangian SPH formulation, two approaches are proposed:

- comparison with experimental results and the Eulerian SPH to assess the accuracy of the total Lagrangian upon the Eulerian for solid mechanics problems through Taylor impact test.
- comparison with FEM model to assess the thermomechanical formulation through forging example.

8.1. Taylor impact test

Taylor impact test, using Iron rods is carried out at 221 m s^{-1} [30] during 4e-3s. The sizes of the used cylindrical specimens are 7.6 mm in diameter and 25.4 mm in height. This example involves large deformations and a large flow

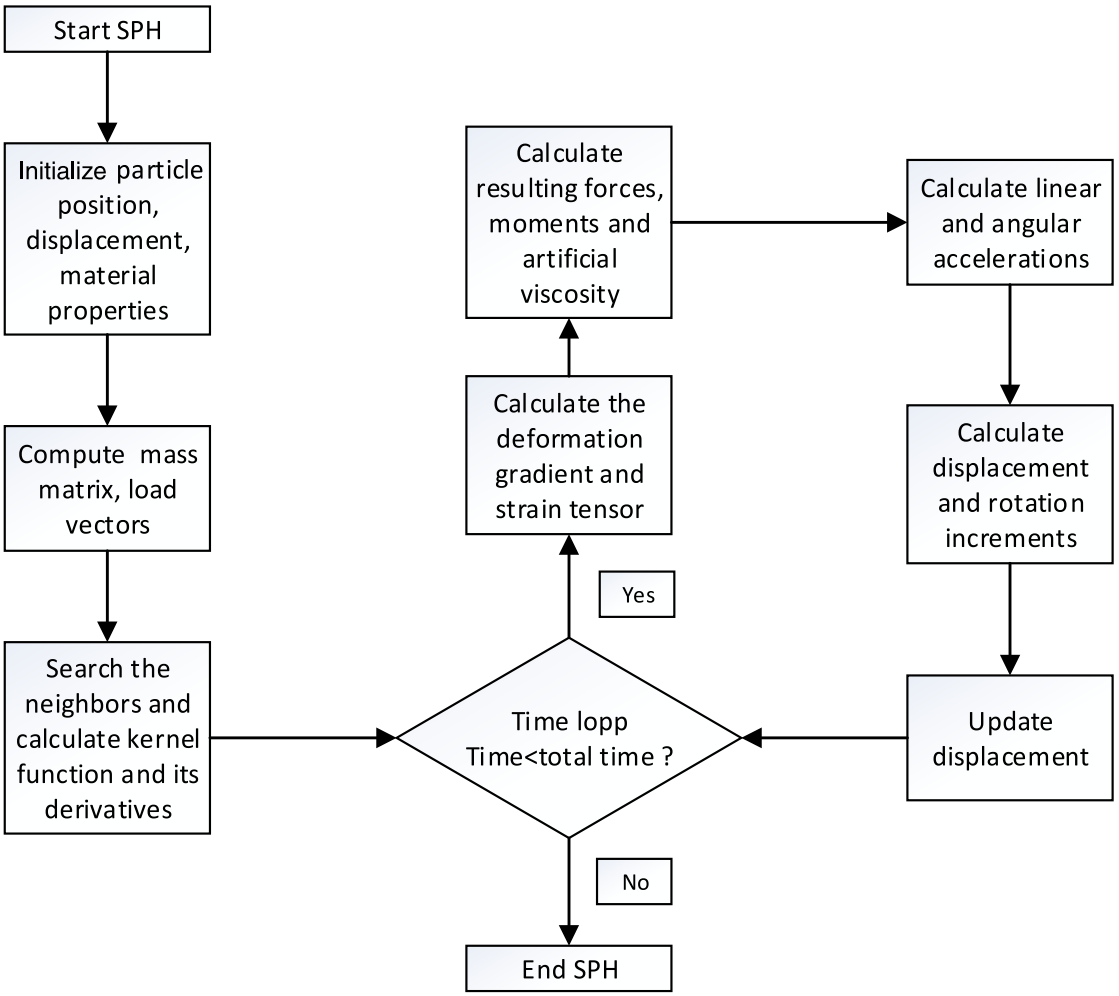

Fig. 4. Flow chart of SPH method.

Table 1
Comparative table of Taylor impact test results after the impact test (see Fig. 8).

	Height H [mm]	Diameter D [mm]	Depth W [mm]	Δ (Error)	Simulation time (s)	Particles
Experimental test [30]	19.8	13.7	8.8	–	–	–
Abaqus—Eulerian	17.53	13.15	9.54	7.96%	336	8608
VUEL—Total Lagrangian	19.35	13.71	8.96	1.39%	23	8608

at the impact interface and 8608 particles are used for the simulation (Fig. 6). The aim of this work is to demonstrate the efficiency of the recently proposed user SPH element through the simulation time and the predicted result in high velocity impact. Results are gathered in Table 1.

The numerical model's performance is obtained by comparing the final diameter, height, and width at 20% of the initial height [39]. Fig. 7 shows the diagram of the part after impact and the equation used to calculate the error is the following:

$$\%error = \frac{1}{3}\left(\frac{|\Delta W|}{W_{test}} + \frac{|\Delta D|}{D_{test}} + \frac{|\Delta H|}{H_{test}}\right) \times 100\% \tag{73}$$

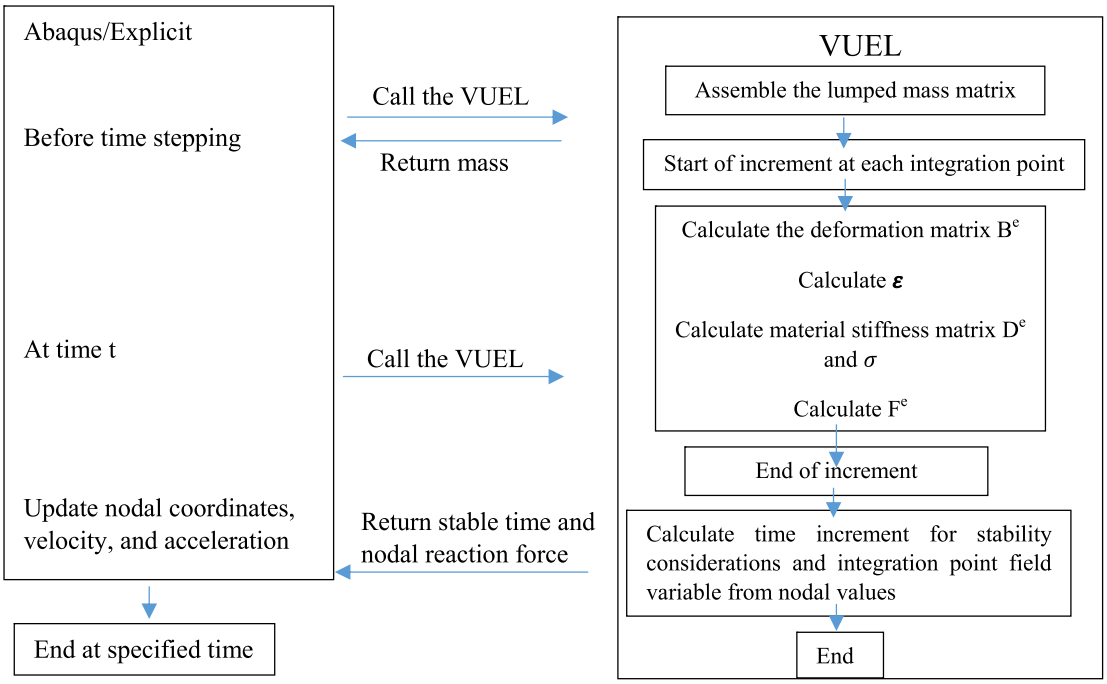

Fig. 5. Logic diagram of the VUEL and flow chart of VUEL subroutine.

Fig. 6. Taylor impact test: Comparison of SPH Abaqus and VUEL.

Very good agreements are found showing the interest of the total Lagrangian SPH formulation for large deformation and high-speed test. In fact, all the dimensions of the deformed sample are very well predicted by the simulation (Table 1), corresponding to a very low percentage of error (1.39%) versus 5.7 times higher in the Eulerian simulation (7.96%). Also, the test shows tensile instability with the Eulerian code and the correction made with the total Lagrangian formulation (Fig. 6) where the kernel is in a Lagrangian formulation. In the Eulerian formulation, the particles move inadequately, precision is lost in the results. In addition, a lower simulation time is found (15 times less), since it is not necessary to update the neighboring particles that remain the same during the simulation.

8.2. Hot forging test

Forging example is simulated using the thermomechanical total Lagrangian SPH formulation in-house code and is compared with FEM (Figs. 8 and 9). Two rigid bars are deforming a deformable body at constant velocity. The block is made in aluminum 7000 series and its initial temperature is 400 ° C. The velocity of the rigid bars is 1 mm s^{-1}.

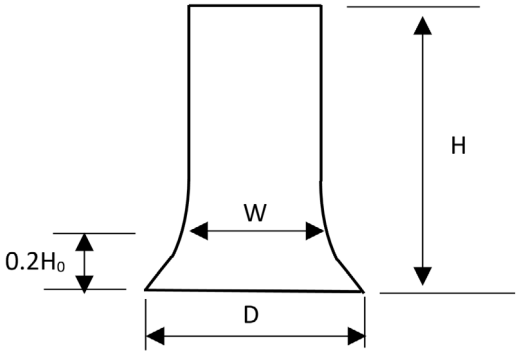

Fig. 7. Deformed sample.

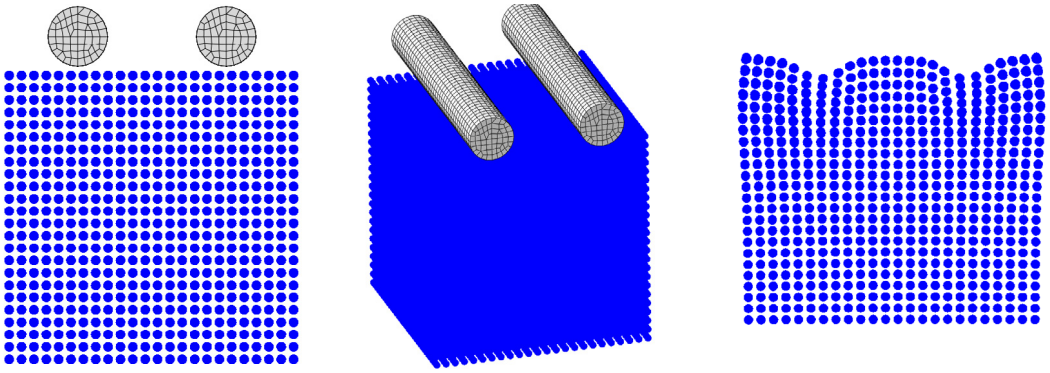

Fig. 8. SPH simulation.

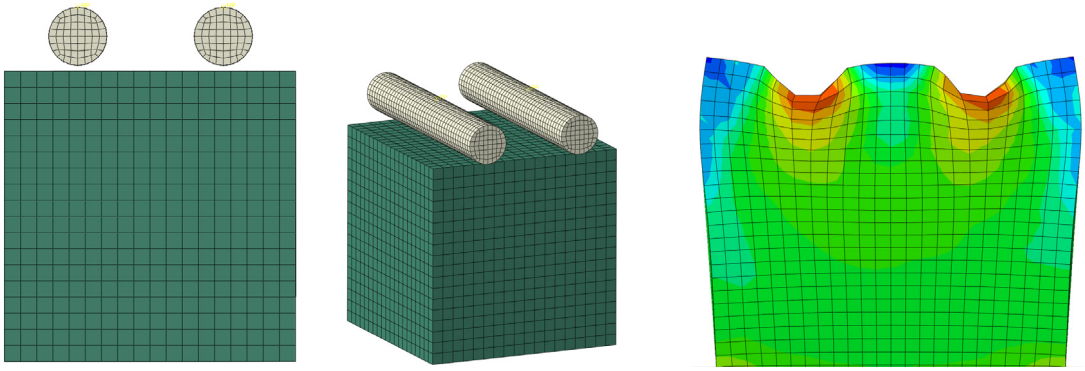

Fig. 9. FEM simulation.

Stress–strain and temperature curves at the maximum stress concentration are shown in Figs. 10 and 11.

As for the Taylor impact test, the forging test shows very interesting results. The performance of the SPH code is remarkable toward the FEM simulation. Comparison of the results shows low discrepancies, 1.31% for the stress–strain curve and 5.17% for the temperature curve. The thermomechanical coupling is then accurate. In addition, the

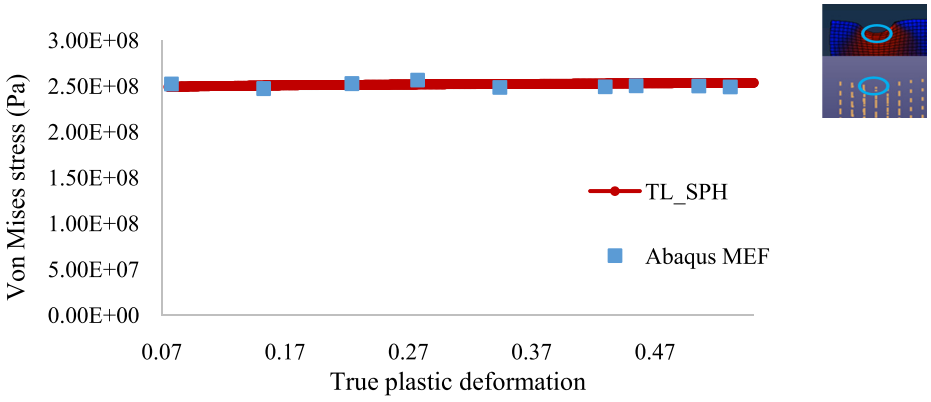

Fig. 10. Stress–strain curve.

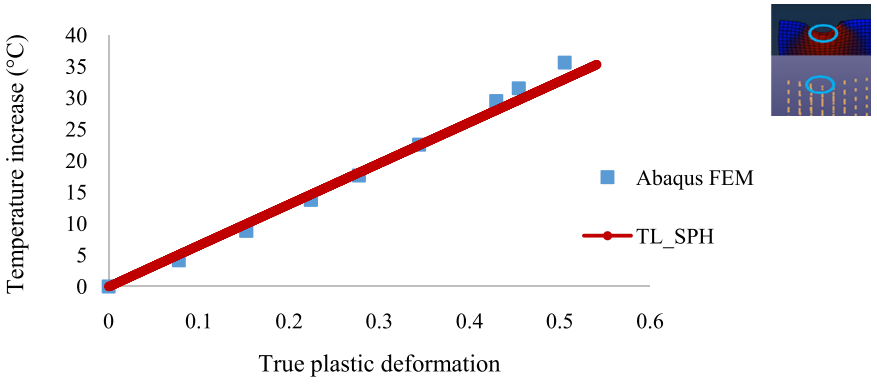

Fig. 11. Temperature increase curve.

SPH simulated part has smoother contours (particles are well ordered) showing no distortion while the FEM example already shows rougher contours that will lead to higher distortions and mesh problems.

9. Conclusion

A thermomechanical SPH in total Lagrangian formulation was proposed to simulate large deformations problems. A corrected particle approximation within an energy-based framework is used for a better representation. Drawbacks such as lack of completeness and interpolation consistency are corrected.

In order to evaluate the performance of total Lagrangian formulation, a Taylor impact test and a forging test were developed. The findings show that the total Lagrangian SPH formulation is of great interest to simulate a thermomechanical process in SPH solid mechanics such as forging or machining: temporal and numerical drawbacks (tensile instability) are corrected. In addition, good precision are found comparing with FEM.

Future works will be to investigate the correction of the zero energy modes through the technique of the hourglass mode and to compare the total Lagrangian formulation with an updated Lagrangian formulation when extreme deformation are involved and particles need to be updated occasionally.

Acknowledgments

The authors wish to acknowledge Mohamed JEBAHI, Maître de conferences, Laboratoire d'étude des microstructures et de mécanique des matériaux LEM3 – UMR CNRS 7239 for this appreciated help. The authors would also like to acknowledge the financial support from the Natural Sciences and Engineering Research council of Canada (NSERC) and from Heroux-Devtek inc. in the course of this work.

References

[1] T.P. Fries, H.G. Matthies, Classification and Overview of Meshfree Methods, Technical University Braunschweig, Brunswick, Germany, 2004.
[2] S. Li, W.K. Liu, Meshfree and particle methods and their applications, Appl. Mech. Rev. 55 (1) (2002).
[3] G.R. Liu, M.B. Liu, Smoothed Particle Hydrodynamics, A Meshfree Particle Method, Livre, Springer, 2005.
[4] L. Libersky, A. Petschek, T. Carney, J. Hipp, F. Allahdadi, High strain Lagrangian hydrodynamics, J. Comput. Phys. 109 (1993) 67–75.
[5] S. Wolf, Méthode Sans Maillage. Laboratoire de Mathématiques Appliquées Aux Systèmes, 2007.
[6] J.J. Monaghan, Smoothed Particle Hydrodynamics, Monash University, Clayton, Victoria 3168, Australia, 1992.
[7] J.J. Monaghan, Smoothed particle hydrodynamics, Ann. Rev. Astron. Astrophys. 30 (1992) 543–574.
[8] J.J. Monaghan, SPH without a tensile instability, J. Comput. Phys. (ISSN: 0021-9991) 159 (2) (2000) 290–311.
[9] J.J. Monaghan, Smoothed Particle Hydrodynamics, Monash University, Clayton, Victoria 3800, Australia, 2005.
[10] J.L. Lacome, Smooth Particle Hydrodynamics (SPH), A new feature in LS-DYNA, in: Proceedings of the 7th International LS-DYNA Users Conference, 2002.
[11] L. Libersky, A. Petschek, Smooth particle hydrodynamics with strength of materials, in: Advances in the Free-Lagrange Method Including Contributions on Adaptive Gridding and the Smooth Particle Hydrodynamics Method, Springer, 1991, pp. 248–257.
[12] P.W. Cleary, M. Prakash, R. Das, J. Ha, Modelling of metal forging using SPH, Appl. Math. Model. 36 (2012) 3836–3855.
[13] J. Limido, C. Espinosa, Modélisation numérique de la coupe orthogonale en ugv, in: National Conference Proceedings, 2005.
[14] J. Limido, C. Espinosa, M. Salaun, J.L. Lacome, SPH method applied to high speed cutting modelling, Int. J. Mech. Sci. 49 (7) (2007) 898–908.
[15] J. Limido, Étude de l'effet de l'usinage grande vitesse sur la tenue en fatigue de pièces aéronautiques (thèse de doctorat), Université de Toulouse, 2008.
[16] A. Timesli, Simulation du soudage par friction et malaxage à l'aide de méthodes sans maillage (Ph.D. dissertation), Université de Lorraine, 2013.
[17] G. Johnson, S. Beissel, Normalized smoothing functions for SPH impact computations, Internat. J. Numer. Methods Engrg. 39 (16) (1996) 2725–2741.
[18] C.T. Dyka, P.W. Randles, R.P. Ingel, Stress points for tension instability in SPH, Internat. J. Numer. Methods Engrg. 40 (1997).
[19] P. Randles, L. Libersky, Normalized SPH with stress point, Internat. J. Numer. Methods Engrg. 48 (2000) 1445–1462.
[20] G.C. Ganzenmüller, M. Sauer, M. May, S. Hiermaier, Hourglass control for smooth particle hydrodynamics removes tensile and rank-deficiency instabilities, Eur. Phys. J. Spec. Top. 225 (2) (2016) 385–395.
[21] G. Dilts, Moving-least-squares-particles hydrodynamics I, Consistency and stability, Internat. J. Numer. Methods Engrg. 44 (8) (1999) 1115–1155.
[22] J. Chen, J. Beraun, C. Jih, An improvement for tensile instability in smoothed particle hydrodynamics, Comput. Mech. 23 (4) (1999) 279–287.
[23] T. Belytschko, Y. Guo, W.K. Liu, S.P. Xiao, A unified stability analysis of meshless particle methods, Internat. J. Numer. Methods Engrg. 48 (2000) 1359–1400.
[24] A. Farrokhpanah, M. Bussmann, J. Mostaghimi, New smoothed particle hydrodynamics (SPH) formulation for modeling heat conduction with solidification and melting, Int. J. Comput. Methodol. 71 (4) (2017).
[25] Y. Vidal, J. Bonet, A. Huerta, Stabilized updated Lagrangian corrected SPH for explicit dynamic problems, Internat. J. Numer. Methods Engrg. 69 (13) (2007) 2687–2710.
[26] M. Canadija, J. Mosler, On the thermomechanical coupling in finite strain plasticity theory with non-linear kinematic hardening by means of incremental energy minimization, Int. J. Solids Struct. 48 (2011) 1120–1129.
[27] J. Mosler, O.T. Bruhns, On the implementation of rate-independent standard dissipative solids at finite strain –variational constitutive updates, Comput. Methods Appl. Mech. Engrg. (2009). http://dx.doi.org/10.1016/j.cma.2009.07.006.
[28] J. Bonet, M.X. Rogríguez-Paz, Hamiltonian formulation of the variable-h SPH equations, J. Comput. Phys. 209 (2005) 541–558.
[29] J. Bonet, S. Kulasegaram, M.X. Rodriguez-Paz, M. Profit, Variational formulation for the smooth particle hydrodynamics (SPH) simulation of fluid and solid problems, Comput. Methods Appl. Mech. Engrg. 193 (2004) 1245–1256.
[30] M.A. Lavoie, A. Gakwaya, M. Nejad Ensan, Variable-h and energy conserving sph formulation with application in aerospace engineering, J. Math. Eng. Sci. Aerosp. 1 (1) (2010) 27–70.
[31] J. Reveles, Development of a Total Lagangian SPH Code for the Simulation of Solids under Dynamic Loading (Ph.D. dissertation), Cranfield University, 2007.
[32] R. Vignjevic, Review of development of the smooth particle hydrodynamics (SPH) method, Predict. Model. Dyn. Process. (2009) 367–396.
[33] J.D. Anderson, Computational Fluid Dynamics: The Basics with Applications, MeGraw-Hill, 1995.
[34] C. Hirsch, Numerical Computation of Internal and External Flows, vol. 1, Wiley- Interscience publication, 1988.
[35] Abaqus documentation v6.14.
[36] L. Goffin, Development of a Didactic SPH Model, Maitrise, Université de Liège, 2013.
[37] C. Loosveldt, D. Watrin, Alternative Numerical Methods in Continuum Mechanics, Smoothed Particle Hydrodynamics, Université de Liège, 2010.
[38] V. Spingel, High Performance Computing and Numerical Modeling, Lecture 4, Universitat Heidelberg, 2013.
[39] T. Holmquist, G. Johnson, Determination of constants and comparison of results for various constitutive models, J. Phys. IV Colloque 01 (C3) (1991) C3-853-C3-860. http://dx.doi.org/10.1051/jp4:19913119. <jpa-00249922>.